American Mineralogist, Volume 91, pages 1794–1801, 2006

Titanium incorporation and $^{VI}Ti^{3+}$ -$^{IV}Ti^{4+}$ charge transfer in synthetic diopside

HENRIK SKOGBY,[1,*] ULF HÅLENIUS,[1] PER KRISTIANSSON,[2] AND HARUO OHASHI[3]

[1]Department of Mineralogy, Swedish Museum of Natural History, Box 50007, SE-104 05 Stockholm, Sweden
[2]Department of Nuclear Physics, Lund Institute of Technology, Lund University, Box 118, SE-221 00 Lund, Sweden
[3]Hashi Institute for Silicate Science, Nishinakanobu 1-9-25, Shinagawa, Tokyo 142-0054, Japan

ABSTRACT

A series of Ti-doped diopside samples synthesized by fluxgrowth methods under reducing conditions were investigated by microanalytical methods and optical absorption spectroscopy, to assess Ti incorporation mechanisms, valence states, and related electronic transitions. Chemical characterization show that Ti occurs both in the tri-and tetravalent states, with Ti^{4+} preferentially ordered to the tetrahedral position whereas Ti^{3+} is restricted to the M1 position. Charge-balance is maintained by incorporation of Na and minor B, stemming from the flux compound. Polarized optical absorption spectra reveal three major absorption features. Two relatively narrow bands centered at 18 500 and 15 700 cm^{-1}, mainly polarized in the crystallographic **c**-direction, display absorbance values that correlate with the calculated Ti^{3+} (M1) concentration, and are assigned to spin-allowed d-d transitions in Ti^{3+}. A broader band centered around 24 500 cm^{-1} displays absorbance values that are well correlated with the product of $^{VI}Ti^{3+}$ and $^{IV}Ti^{4+}$. Based on the spectral characteristics of this band, including a strong polarization in the crystallographic **b**-direction, we assign this band to an $^{M1}Ti^{3+}$-$^{T}Ti^{4+}$ intervalence charge transfer process.

Keywords: Crystal synthesis, diopside, optical spectroscopy, pyroxene, major and minor elements, Ti in pyroxene, order-disorder

INTRODUCTION

Titanium normally occurs in the tetravalent state in terrestrial minerals, whereas the presence of Ti in the trivalent state is known from the more reduced environments representative for lunar rocks and meteorites. Pyroxenes from occurrences containing Ti^{3+} have earlier been studied by optical absorption spectroscopy (OAS), but the scarcity of good-quality samples of relatively simple compositions has made the interpretation of the spectral features difficult. The studied samples have almost invariably contained additional cations of Fe, which increases the number of possible interactions that have to be considered to cause absorption in the UV-VIS range. These interactions include single-ion d-d transitions in the ions Fe^{2+}, Fe^{3+}, and Ti^{3+}, as well as charge-transfer interactions involving Fe^{2+}-Fe^{3+}, Fe^{2+}-Ti^{4+}, and Ti^{3+}-Ti^{4+} pairs. An exceptional sample in this respect has been the virtually Fe-free but Ti-rich "fassaite" (calcic subsilicic titanoan aluminian pyroxene) from the Allende meteorite, which has been investigated in several OAS studies (Dowty and Clark 1973a, 1973b; Burns and Huggins 1973; Mao and Bell 1974). The causes of the absorption bands in spectra of this sample has been debated, and the spectral features were reinterpreted by Strens et al. (1982) to be caused by electronic transitions involving Ti^{3+} single-ions, exchange-coupled Ti^{3+}-Ti^{3+} pairs, and Ti^{3+}-Ti^{4+} charge transfer.

The aim of this study was to investigate substitutional mechanisms connected with Ti^{3+} and Ti^{4+} incorporation in clinopyroxene, and to further explore the possible electronic transitions involving Ti^{3+} in the diopside structure by OAS. For these purposes, a series of diopside single-crystal samples with different Ti contents and Ti^{3+}/Ti^{4+} ratios were synthesized by flux-growth methods under low oxygen fugacities. In addition, single crystals of a synthetic end-member $NaTiSi_2O_6$ clinopyroxene (Ohashi et al. 1982) were studied for reference purposes.

EXPERIMENTAL METHODS

Crystal synthesis and sample preparation

The diopside single crystals investigated in this study were produced by the flux growth technique using $Na_2B_4O_7$ as a flux compound. The diopside components were weighed out as oxides (analytical grade powders), which were mixed with the flux compound in proportions that allowed the oxides to dissolve at the highest temperature of the experiment. About 5 g of these mixtures were thoroughly ground and transferred to 15 mL platinum crucibles, which were covered by lids. The crucibles were suspended in a vertical tube furnace equipped with a gas-flow system. The typical time-temperature path of the experiments consisted of a relatively fast rise in temperature to 1100 °C, a 24 hour plateau at this temperature to allow dissolution and homogenization, and then a linear cooling path of 2 or 4 °/h down to 700 °C, from which the samples were allowed to cool more quickly down to room temperature. Before the temperature plateau was reached, an H_2-CO_2 gas flow was started, with H_2:CO_2 proportions in the range 1:1 to 5:1, which correspond to log f_{O_2} values equal to +0.5 to –1 relative to the Fe-wüstite solid buffer. The oxygen fugacity during the runs was monitored via a zirconia electrolyte sensor. The synthesis products consisted of many euhedral diopside single crystals embedded in residual glass. The diopside single crystals were recovered after dissolving the glass phase in warm diluted HCl. The crystals are elongated along the **c**-axis with dimensions up to $1 \times 1 \times 5$ mm and are normally clear but contain occasional cracks and minor melt inclusions. The Ti-doped crystals range in color from gray to grayish brown. For the most Ti-rich compositions (Di-80 and Di-72), rod-shaped rutile crystals are abundant. The size of the rutile crystals varies, from a few to 100 μm in the smallest dimension and lengths from 30 μm to 3 mm.

* E-mail: henrik.skogby@nrm.se

0003-004X/06/1112–1794$05.00/DOI: 10.2138/am.2006.2154

Single crystals free of inclusions, or with large inclusion-free parts, were selected for the analytical and spectroscopic studies. Sample preparation consisted of crystallographic orientation by aid of the developed (110) and (010) surfaces and optical methods, embedding in plastic resin, and polishing on parallel surfaces. The same crystals were then used for the microchemical analysis as well as the spectroscopic measurements.

Microprobe analysis

The concentration of the heavier elements was determined by electron microprobe analysis, whereas B was analyzed by a nuclear microprobe at Lund Institute of Technology. The electron microprobe analyses were carried out on a Cameca SX50 instrument operated at 20 kV accelerating potential and 12 nA sample current, with albite (Si, Na), MgO (Mg), $MnTiO_3$ (Ti), and wollastonite (Ca) as standard materials. Sodium data were always measured in the first analytical cycle, to minimize potential elemental loss. The raw analytical data were reduced using the ZAF-related PAP program (Pouchou and Pichoir 1984). Five to ten points were analyzed for each sample in the areas used for the optical spectroscopic measurements.

Boron was analyzed using a focused proton beam, utilizing the broad resonance of the $^{11}B(p,\alpha)2\alpha$ nuclear reaction around 660 keV. The analyses were performed by scanning the proton beam over the same areas as used for the optical absorption measurements. To normalize data, tourmaline was used as a standard. This technique, which has been described in detail elsewhere (Kristiansson et al. 1999; Hålenius et al. 2000; Skogby et al. 2003), has an estimated detection limit of 10 ppm and an estimated relative analytical error of 5–10%.

To verify that sub-micrometer phases were not present in the flux-grown samples, some crystals were examined by transmission electron microscopy using a JEOL 2000 FX instrument operated at 200 kV and equipped with a LINK AN1000 EDS system at the Department of Inorganic Chemistry, Stockholm University. The crystals were studied with a point to point resolution of 0.4 nm and an analytical spatial resolution of 40 nm.

Optical absorption spectroscopy

Optical absorption spectra were acquired at ambient conditions in the UV-VIS range (300–800 nm) using a Zeiss MPM 800 microscope spectrometer at the Swedish Museum of Natural History. A75-W xenon arc lamp was used as the light source, concave gratings as the monochromator, and a photomultiplier as the detector. Zeiss Ultrafluar 10× lenses were used as the condenser in all measurements. Doubly polished, oriented single crystals served as absorbers, with the analyzed areas masked by aid of circular apertures with diameters in the range 40–100 μm to avoid occasional cracks and flux inclusions. Sample thicknesses were measured with a digital micrometer and varied between 35 and 222 μm. The spectra were obtained in polarized mode using a Glan-Thompson prism and a spectral slit width of 1 or 2.5 nm. Diopside single crystals were measured in the E||Y (crystallographic **b**-direction) and E||**c** directions on (100) crystal sections. Additional directions were measured on crystals oriented parallel to (010), and perpendicular to the **c**-axis, for some samples. Polarized single-crystal spectra of the end-member $NaTiSi_2O_6$ clinopyroxene were obtained on polished (010) and (001) sections, from which E||X, E||Z, and E||Y-spectra were obtained, respectively. The different choice of crystallographic absorber orientations for the flux-grown diopside crystals and the end-member NaTi-clinopyroxene is based on the fact that their optical indicatrix axes bear a different relationship to the crystallographic axes. In the diopside crystals, the angle between the optical X-axes and the crystallographic c-axes is ca. 45° (Fig. 1), whereas this angle is strongly reduced to ca. 7° in the $NaTiSi_2O_6$ end-member.

To quantify the absorption data, the spectra were analyzed by aid of a fitting software (Jandel PeakFit) using Gaussian band shapes, and applying several constraints described below.

RESULTS

Chemistry

The data obtained from the microprobe analyses and the calculated structural formulae are given in Table 1. In the present series of flux-grown diopside samples, TiO_2 contents range from 2.8 to 11.8 wt%. Moreover, all samples take up small amounts of Na and B from the flux compound. Several crystals show a marked zonation with Ti-poor cores and Ti-rich edges, with a difference in Ti content commonly around 30%. The structural formulae were calculated using the following procedure: the number of cations was normalized to four, and the Ti^{3+}/Ti^{4+} ratio was then adjusted to obtain charge neutrality. The tetrahedral position was filled by allocating Si, B, and Ti^{4+}, and remaining Ti^{4+}, Ti^{3+}, and Mg were allocated to fill the M1 position. Finally Na, Ca, and any remaining Mg, were confined to the M2 position. All samples show an Si deficiency that is only partly compensated by the small amounts of B, and thus Ti^{4+} also seems to enter the tetrahedral position. Although most of the tetravalent Ti is ordered to the tetrahedral position, trivalent Ti is restricted to the M1 position. The Ti^{3+}/Ti_{tot} ratios for the studied samples vary from 0.18 to 0.77. The end-member reference crystal is characterized chemically by a virtually ideal $NaTiSi_2O_6$-composition indicating that Ti is present in the trivalent state at the six-coordinated M1-site.

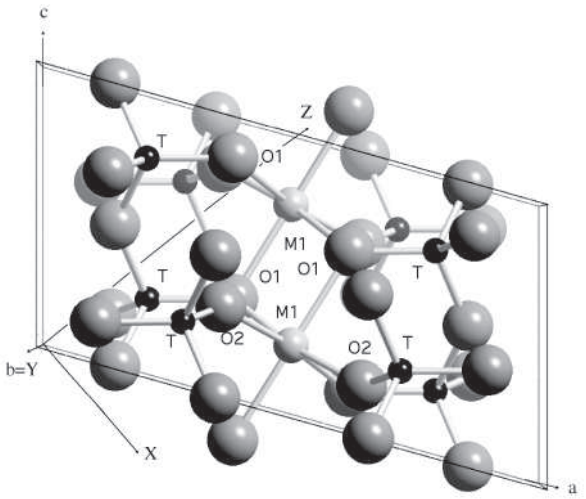

FIGURE 1. Perspective projection of the diopside structure close to (010) showing part of the *C*2/*c* clinopyroxene crystal structure and the relationship between the optical directions X, Y, Z and the crystallographic axes **a**, **b**, and **c**. The optical X- and Z-directions lie in the crystallographic **a-c** plane.

Optical absorption spectroscopy

Polarized optical absorption spectra obtained on oriented sample sections of the Ti-doped diopside crystals reveal three major absorption features; one broad band ($\omega_{1/2} \approx 8500$ cm^{-1}) centered around 24 500 cm^{-1} (408 nm) being strongly polarized in the Y-direction, and two more narrow ($\omega_{1/2} \approx 2500$ cm^{-1}) bands centered at 18 500 cm^{-1} (541 nm) and 15 700 cm^{-1} (637 nm) mainly polarized in the crystallographic **c**-direction (E||**c**), as shown in Figure 2. All three bands show intermediate absorption intensity in the E||X and E||Z directions. Because the bands were strongly polarized in E||Y and E||**c**, the study concentrated on these directions, with spectra collected on the same (100) section for each sample. The resultant spectra are plotted in Figure 3a (E||Y) and Figure 3b (E||**c**). In contrast, the spectra (E||X, E||Y, and E||Z) of the $NaTiSi_2O_6$ crystals lack the broad absorption band at ca. 24 500 cm^{-1}, but the two relatively narrow (ca. 2500 cm^{-1}) and intense bands at ca. 18 700 cm^{-1} and ca. 15 700 cm^{-1} recorded in spectra of the diopside crystals are also evident here (Fig. 4).

TABLE 1. Microprobe analysis of synthetic clinopyroxene

Sample	Di-68	Di-64	Di-55	Di-81b	Di-63	Di-65	Di-81a	Di-66a	Di-66b	Di-73	Di-80	Di-72	R5
H_2:CO_2*	air	5:1	1:1	1:1	2:1	5:1	1:1	5:1	5:1	5:1	1:1	5:1	Belt type
B_2O_3	0.05(1)	0.29(3)	0.30(3)	0.15(2)	0.32(3)	0.30(3)	0.45(5)	0.52(5)	0.44(5)	0.38(4)	0.34(4)	0.67(7)	–
Na_2O	0.1(1)	0.9(1)	0.9(1)	1.2(4)	1.1(1)	1.3(1)	1.3(1)	1.6(2)	1.6(1)	1.8(3)	2.4(1)	3.0(1)	13.5(4)
MgO	19.0(2)	17.6(2)	17.9(1)	16.9(6)	17.0(2)	16.8(2)	16.3(2)	16.0(2)	16.3(3)	16.8(4)	15.3(1)	13.6(2)	–
SiO_2	55.0(10)	54.2(3)	53.9(4)	53.3(4)	53.2(3)	52.8(4)	52.6(5)	52.9(7)	52.4(5)	52.4(6)	51.9(3)	50.7(6)	54.8(3)
CaO	25.7(3)	24.6(2)	24.2(2)	23.0(8)	23.9(1)	23.7(1)	23.2(1)	22.5(4)	22.6(1)	21.9(3)	20.6(1)	19.5(2)	–
TiO_2	0.00(0)	2.8(1)	3.1(3)	4.4(9)	4.6(1)	5.2(1)	6.2(1)	6.8(5)	7.1(3)	7.1(3)	9.5(1)	11.8(6)	32.1(1)†
sum	99.8	100.4	100.3	99.0	100.2	100.1	100.1	100.3	100.5	100.4	100.0	99.3	100.6
Cation distribution													
T- site													
B	0.003	0.018	0.019	0.009	0.020	0.019	0.028	0.033	0.028	0.024	0.022	0.043	–
Si	1.978	1.952	1.939	1.954	1.928	1.918	1.918	1.924	1.902	1.899	1.902	1.881	2.016
Ti^{4+}	–	0.030	0.043	0.036	0.052	0.064	0.054	0.043	0.071	0.077	0.076	0.076	–
sum	1.982	2.000	2.000	2.000	2.000	2.000	2.000	2.000	2.000	2.000	2.000	2.000	2.016
M1 site													
Mg	1.000	0.944	0.959	0.915	0.918	0.910	0.885	0.857	0.878	0.884	0.815	0.745	–
Ti^{3+}	–	0.013	0.000	0.072	0.049	0.045	0.106	0.143	0.101	0.082	0.180	0.252	0.993
Ti^{4+}	–	0.033	0.041	0.013	0.025	0.032	0.008	0.000	0.021	0.034	0.005	0.003	–
sum	1.000	0.990	1.000	1.000	0.992	0.987	1.000	1.000	1.000	1.000	1.000	1.000	0.993
M2 site													
Na	0.006	0.062	0.066	0.089	0.079	0.090	0.095	0.110	0.115	0.127	0.168	0.215	0.990
Ca	0.991	0.947	0.933	0.904	0.929	0.922	0.905	0.878	0.880	0.849	0.810	0.776	–
Mg	0.020	0.000	0.002	0.007	0.000	0.000	0.001	0.012	0.005	0.024	0.022	0.010	–
sum	1.017	1.009	1.000	1.000	1.008	1.012	1.000	1.000	1.000	1.000	1.000	1.001	0.990

Notes: Numbers within parentheses refer to the estimated relative error for B_2O_3 analysis and the observed standard deviations (1σ) for the analysis of the heavier elements.
* H_2:CO_2 gas mixing ratio during synthesis.
† The Ti content for the $NaTiSi_2O_6$ end-member sample (R5) is given as Ti_2O_3.

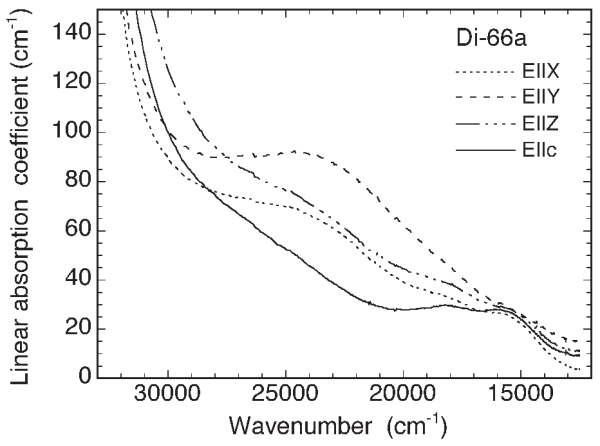

FIGURE 2. Polarizedoptical absorption spectra of Ti-doped synthetic diopside (sample Di-66a, see Table 1).

To determine the individual band absorbance for the three bands, the spectra were modeled using Gaussian peak-fitting software. In the fitting procedure, it became necessary to lock the peak position for the 24 500 cm^{-1} band in the E||**c** and E||Z polarization, where the band is weak, to the position obtained for E||Y where the band is strong. Similarly, the peak positions obtained for the 18 500 cm^{-1} and 15 700 bands for E||**c** were used also for E||Y and E||X. In addition, the widths of the 18 500 cm^{-1} and 15 700 bands were constrained to be equal, as the widths otherwise varied considerably in the fits for the different samples. The UV-edge was modeled by one (E||Y) or two (E||**c**) strong Gaussian bands, with centers outside the measured range, so that the tails of these bands accounted for the obtained UV edge. The result of typical fits are shown in Figure 5 and the individual band absorbances (as α_{net} values) are given in Table 2.

DISCUSSION

Cation distribution and substitution mechanisms

The results from the chemical microanalyses of the flux-grown diopside samples show that a considerable proportion of the Ti occur in the trivalent state, as a result of the strongly reducing atmosphere applied during synthesis. Titanium preferably enters the M1 site in the trivalent state, and the tetrahedral site in the tetravalent state. Together with B, Ti^{4+} compensates for the insufficient amounts of Si in the tetrahedral site, and as can be seen in Figure 6 where both B and Ti are correlated positively with the Si deficiency. The replacement of Mg by Ti^{3+} in the M1 position yields a charge excess of 1, whereas the minor replacement of Mg by Ti^{4+} yields a charge excess of 2. Charge compensation for these substitutions is provided mainly by Na replacing Ca in the M2 octahedral position, and also by B replacing Si in the tetrahedral position. In accordance with this interpretation, the Na and B contents are well correlated with the total Ti content as illustrated in Figure 7. The occurrence of Ti^{4+} and B at the tetrahedral position is supported further by single-crystal XRD and structure refinement studies performed on selected samples of the present study (Nazzareni et al. 2004) and also has been observed previously in natural diopside (Quartieri et al. 1993). The virtually stoichiometric $NaTiSi_2O_6$ end-member is related to diopside by the coupled exchange $^{M2}Na^{+M1}Ti^{3+M2}Ca^{2+}_{-1}{}^{M1}Mg^{2+}_{-1}$.

Absorbance correlations

The absorbance values (α_{net}) observed for the three bands (Table 2) are correlated with the Ti concentrations of the samples.

TABLE 2. Net linear absorption coefficient (α_{net}) and absorber thicknesses for flux grown Ti-diopside

Sample	Di-64	Di-55	Di-81b	Di-63	Di-65	Di-81a	Di-66a	Di-66b	Di-73	Di-80	Di-72
					α_{net} (cm^{-1})						
15700, E‖**c**	5.7	2.2	8.7	11.4	13.5	11.6	16.3	18.3	15.6	18.5	30.8
18500, E‖**c**	4.2	1.8	7.0	9.1	10.7	9.2	12.9	13.1	11.0	16.3	24.5
24500, E‖Y	9.2	5.4	22.8	31.5	32.5	42.1	75.8	82.9	93.4	96.9	202
Thickness (µm)	74	222	134	151	118	143	102	78	41	45	35

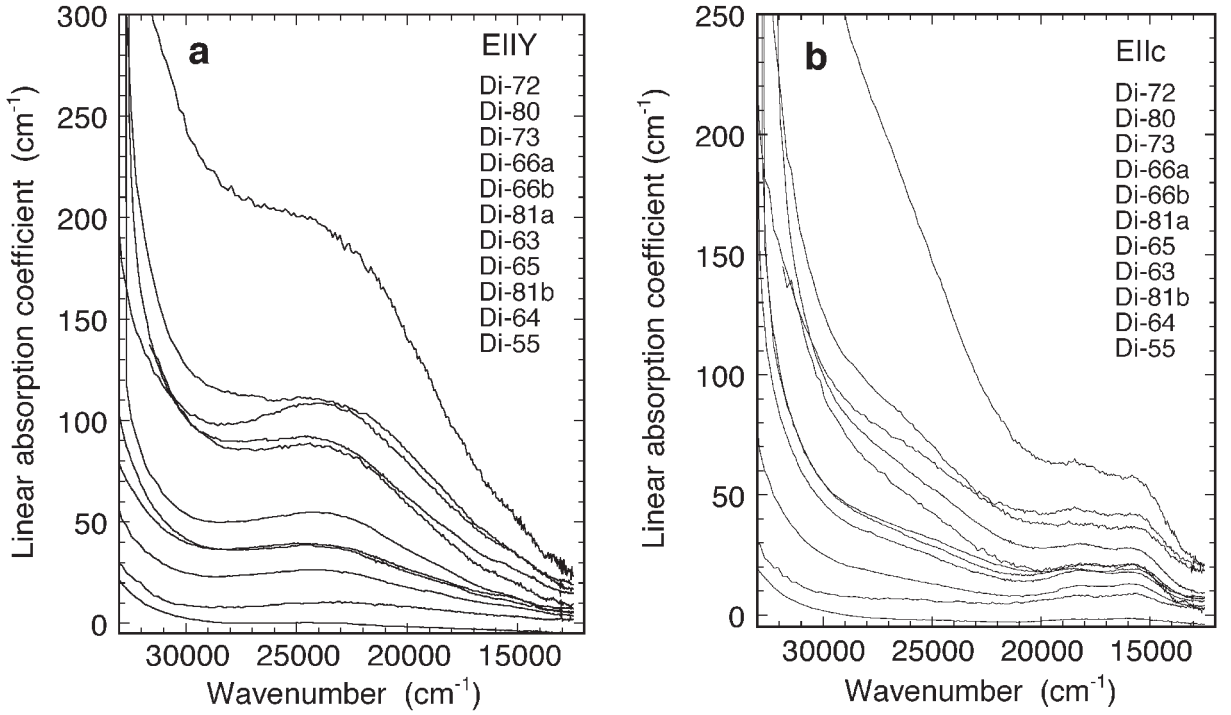

FIGURE 3. Optical absorption spectra polarized in the Y-direction (**a**) and crystallographic **c**-direction (**b**) of synthetic diopside samples with different Ti contents (see Table 1). Spectra were obtained on (100) sections, are offset for clarity, and plotted from top to bottom as listed in legends.

In Figures 8a and 8b, the net linear absorption coefficients (α_{net}) obtained by peak fitting of the 15 700 and 18 500 cm^{-1} bands in the E‖**c** direction have been plotted against the calculated Ti^{3+} concentration in the M1 position. Pronounced correlations are observed (r^2 = 0.87 and 0.90, respectively), although scatter of the data points is present. The scatter can be ascribed mainly to the uncertainty in calculated Ti^{3+} contents, which were obtained by applying charge-balance considerations of the structural formulae based on the microprobe analyses, but also to the observed compositional zonation. The regression lines shown in the plots do not intersect the origin, which indicate that the baseline fitting procedure did not fully reproduce the true baseline.

The α_{net} values for the 24 500 cm^{-1} band in the E‖Y direction show a good correlation with the product of $^{VI}Ti^{3+}$ and $^{IV}Ti^{4+}$ (Fig. 8c). Linear regression of the data give a correlation coefficient of r^2 = 0.90. The reasons for the observed scatter can be assumed to be the same as for the 15 700 and 18 500 cm^{-1} bands.

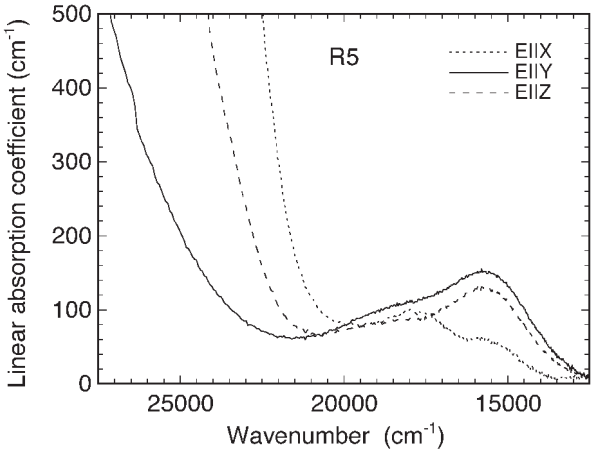

FIGURE 4. Optical absorption spectra of synthetic $NaTiSi_2O_4$ end-member pyroxene (R5; see Table 1) polarized in the X, Y, and Z directions.

Spectrum interpretation and band assignments

Published spectra of natural Ti^{3+}-bearing clinopyroxenes ("fassaite") reveal three absorption bands at ca. 21 500, 16 100, and 14 000 cm^{-1} (Burns and Huggins 1973; Dowty and Clark 1973a, 1973b; Mao and Bell 1974). The absorption band at 21 500 cm^{-1} has invariably been assigned to a spin-allowed d-d transition in Ti^{3+} at the M1-site. The band at ca. 14 000 cm^{-1} was observed only in spectra recorded by Mao and Bell (1974), who assigned it to a Ti^{3+}-Ti^{4+} intervalence charge transfer (IVCT) pro-

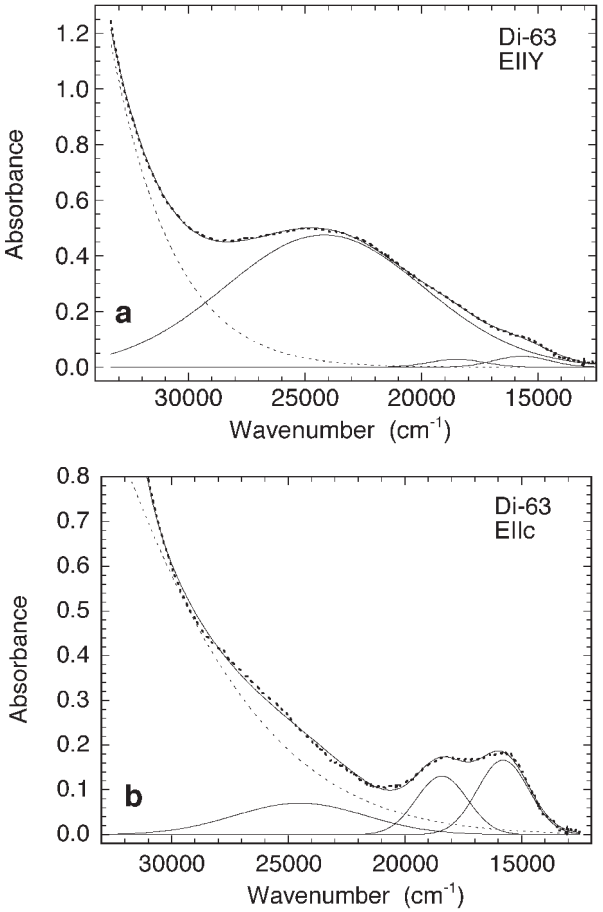

FIGURE 5. Example of spectral fitting for Ti-doped diopside spectra. (**a**) Spectrum polarized in the Y-direction obtained on a (100) section. (**b**) Spectrum polarized along the **c**-direction obtained on a (100) section. Thick dashed lines indicate mesured spectra, thin dashed lines indicate fitted UV background absorption. Absorber thickness = 151 µm.

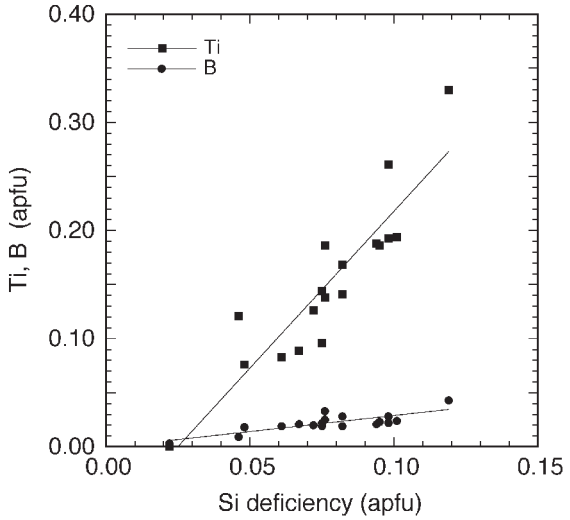

FIGURE 6. Contents of Ti and B plotted vs. Si deficiency for synthetic diopside samples. The data set includes samples in addition to those listed in Table 1.

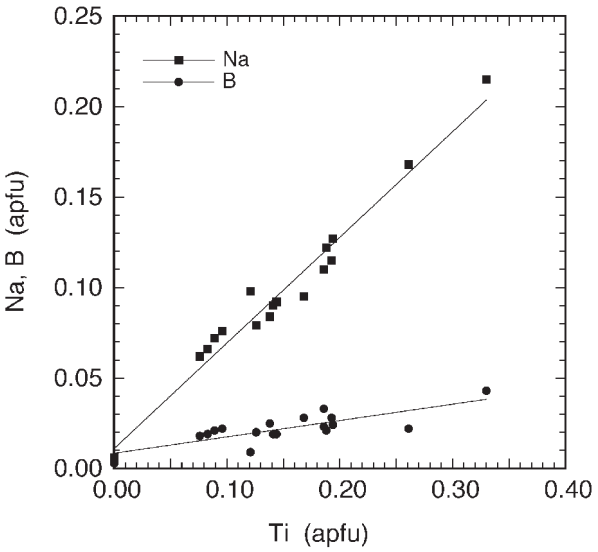

FIGURE 7. Contents of Na and B plotted vs. Ti content for synthetic diopside samples. The data set includes samples in addition to those listed in Table 1.

cess. Dowty and Clark (1973a, 1973b) assigned the absorption band at ca. 16 500 cm^{-1} to IVCT processes between Ti^{3+} and Ti^{4+} cations at M1-sites. Burns and Huggins (1973) challenged this interpretation and proposed that this band marked a spin-allowed d-d transition to split ^2E_g excited levels in Ti^{3+} at the M1-site. Mao and Bell (1974) supported this latter interpretation. Strens et al. (1982) presented reinterpretations of the fassaite spectra that were, with the exception of a proposed Ti^{3+}-Ti^{3+} pair origin for the band at 16 100 cm^{-1}, in accordance with those proposed by Burns and Huggins (1973) and Mao and Bell (1974).

Diffuse reflectance spectra of synthetic $NaTiSi_2O_6$ presented by Prewitt et al. (1972) shows a weak absorption band at ca. 15 600 cm^{-1} and a strong UV absorption edge, which precludes observations of discrete absorption bands above ca. 20 000 cm^{-1}. They interpreted the 15 600 cm^{-1} band in terms of IVCT processes between Ti^{3+} and Ti^{4+} cations at M1-sites. Burns and Huggins (1973) proposed an alternative assignment of this band to a spin-allowed d-d transition to split ^2E_g excited levels in Ti^{3+} at the M1-site.

15 700 and 18 500 cm^{-1} bands. In the polarized single-crystal absorption spectra of synthetic Ti^{3+}-bearing clinopyroxene, we have recorded two absorption bands at 15 700 and 18 500 cm^{-1}. The band at lower energies coincides with the band noted in diffuse reflectance spectra of $NaTiSi_2O_6$ (Prewitt et al.1972), and it is also energetically close to one of the bands observed in spectra of natural calcic Ti^{3+}-bearing pyroxene crystals. The band at 18 500 cm^{-1} occurs at a distinctly lower energy, ca. 3000 cm^{-1}, than the potential counterpart in the previously reported spectra of the natural crystals. Reasons for this dissimilarity may be that a different electronic process causes the band in the natural samples or that the real structure at the Ti^{3+}-site of the natural samples differs from that in the synthetic ones. The mean Ti^{3+}-O distance in the $NaTiSi_2O_6$ end-member is 2.046–2.054 Å

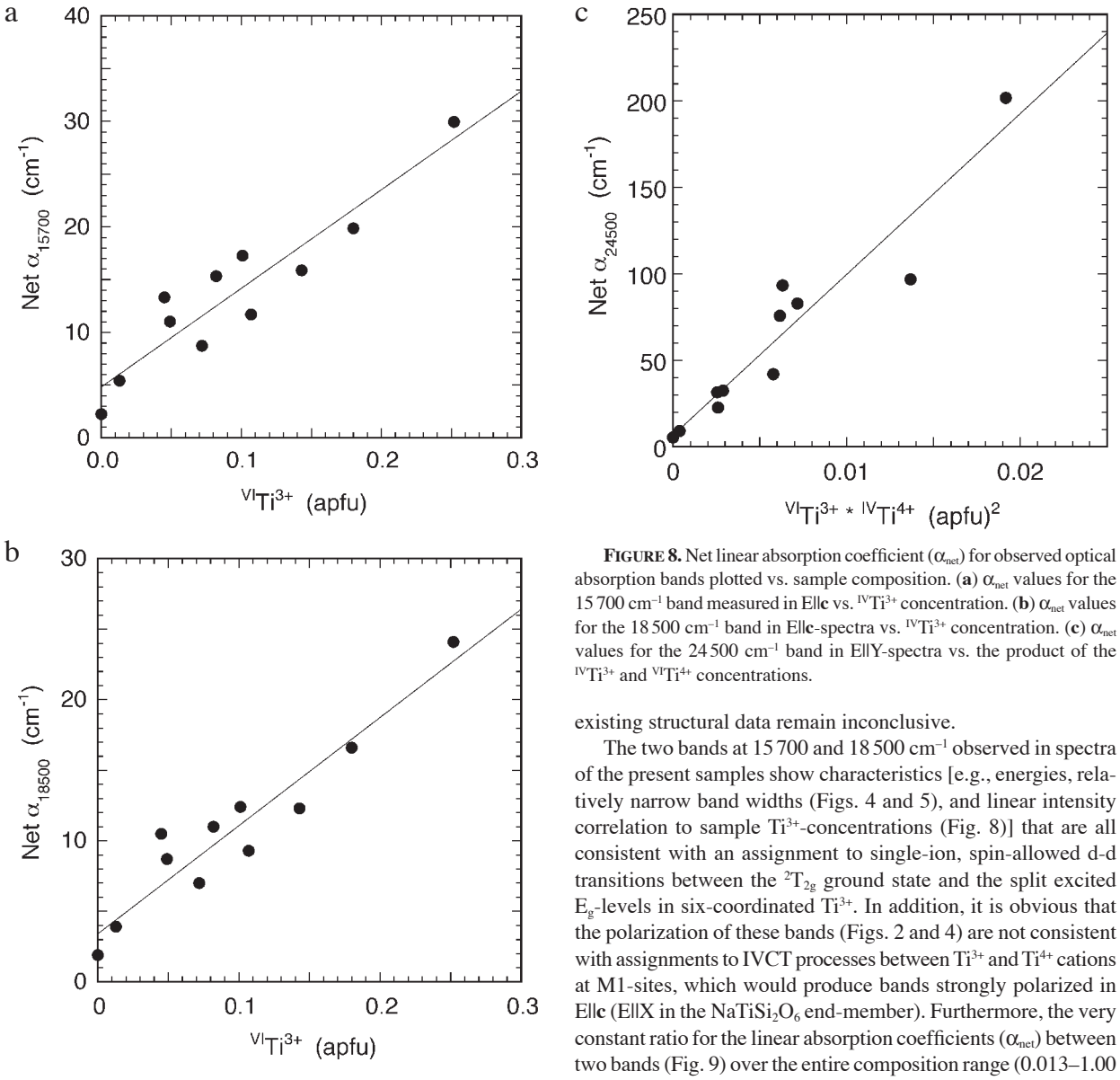

FIGURE 8. Net linear absorption coefficient (α_{net}) for observed optical absorption bands plotted vs. sample composition. (**a**) α_{net} values for the 15 700 cm^{-1} band measured in E||**c** vs. $^{IV}Ti^{3+}$ concentration. (**b**) α_{net} values for the 18 500 cm^{-1} band in E||**c**-spectra vs. $^{IV}Ti^{3+}$ concentration. (**c**) α_{net} values for the 24 500 cm^{-1} band in E||Y-spectra vs. the product of the $^{IV}Ti^{3+}$ and $^{VI}Ti^{4+}$ concentrations.

(Ohashi et al. 1982; Redhammer et al. 2003) whereas the mean M1-O distance in Ti^{3+}-bearing "fassaite" has been determined to be 2.059 Å (Dowty and Clark 1973a). The distortion of the M1-site from O_h-symmetry is similar in the two structures. This result suggests that the crystal-field splitting (10Dq) for Ti^{3+} at the M-site should be larger in the $NaTiSi_2O_6$ end-member than in the natural samples, but the splitting of the excited ^2E_g-state of Ti^{3+} should be similar. In contrast to these predictions, published spectra indicate a larger crystal-field splitting (10Dq = 18 800 cm^{-1} compared to 17 100 cm^{-1}) and larger splitting of the excited state (ca. 5400 cm^{-1} compared to 2800 cm^{-1}) for the natural "fassaite." However, the published mean M1-O distance determined for the "fassaite" with a Ti^{3+}-occupancy of 0.48 at the M1-site represents a mean value, and the real mean Ti^{3+}-O distance may differ depending on the degree of structural relaxation. Consequently, comparisons and interpretations of the previously published spectra of natural samples based solely on existing structural data remain inconclusive.

The two bands at 15 700 and 18 500 cm^{-1} observed in spectra of the present samples show characteristics [e.g., energies, relatively narrow band widths (Figs. 4 and 5), and linear intensity correlation to sample Ti^{3+}-concentrations (Fig. 8)] that are all consistent with an assignment to single-ion, spin-allowed d-d transitions between the $^2T_{2g}$ ground state and the split excited E_g-levels in six-coordinated Ti^{3+}. In addition, it is obvious that the polarization of these bands (Figs. 2 and 4) are not consistent with assignments to IVCT processes between Ti^{3+} and Ti^{4+} cations at M1-sites, which would produce bands strongly polarized in E||**c** (E||X in the $NaTiSi_2O_6$ end-member). Furthermore, the very constant ratio for the linear absorption coefficients (α_{net}) between two bands (Fig. 9) over the entire composition range (0.013–1.00 Ti^{3+} pfu) further underlines that identical electronic processes cause the two bands.

Based on a Ti^{3+}-origin, the maximum molar absorption coefficients (ε) for the bands at 15 700 and 18 500 cm^{-1} in spectra of the $NaTiSi_2O_6$ end-member were calculated to be 6.5 and 5 L/mol·cm, respectively. These numbers compare with maximum ε-values of 9 ± 2 and 7 ± 2 L/mol·cm for the corresponding bands in the flux-grown diopside crystals with total Ti contents in excess of 0.1 apfu. The ε-values of these bands are generally higher in spectra of the flux-grown crystals with lower Ti contents. We ascribe this to the earlier mentioned uncertainties in calculated Ti^{3+} contents for samples with low concentrations of Ti_{tot} and to the imperfect spectral baseline fitting. The observed ε-values for the two bands are consistent with assignments to single-ion, spin-allowed d-d transitions in Ti^{3+} at the M1-site.

24 500 cm^{-1} band. A broad absorption band ($\omega_{1/2} \approx 8500$ cm^{-1}) observed at 24 500 cm^{-1} in the spectra of the present diopside

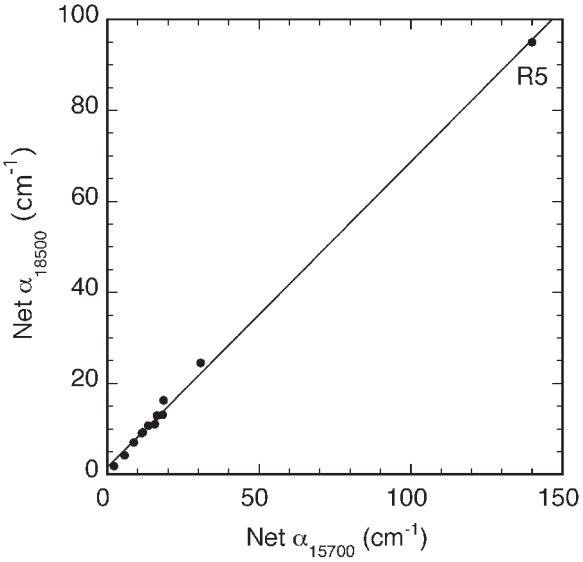

FIGURE 9. Correlation of the net linear absorption coefficient (α_{net}) for the 15 700 and 18 500 cm^{-1} bands. "Net α" indicates the strongest absorption observed in all measured directions. Correlation coefficient $r^2 = 0.998$.

crystals, but not in spectra of the $NaTiSi_2O_6$ end-member, display features commonly associated with IVCT processes. Most conspicuous IVCT characteristics are broad bands ($\omega_{1/2} > 5000$ cm^{-1}) and strong band polarization along structural M-M vectors (e.g., Mattson and Rossman 1987, 1988).

Alternative processes causing broad absorption bands in spectra of oxygen-based mineral structures also have been demonstrated. For instance, absorption in inclusions of submicroscopic solid impurities (dumortierite) been shown to cause absorption bands in spectra of rose-colored quartz (Goreva and Rossman 2000; Goreva et al. 2001; Ma et al. 2002). Mie scattering as the origin for strong and broad absorption bands in the UV-VIS spectral region bands represents an additional effect caused by submicroscopic solid impurities, which has been documented in, for example, absorption spectra of garnets (Khomenko et al. 2002). This effect was discovered and explained by Mie (1908) who showed that wavelength-dependent light scattering by small particles in a homogenous transparent medium depends on the frequency, shape, and size of the inclusions as well as the refractive index of the host medium and the inclusion. Methods for calculations of Mie scattering have been described in detail in Bohren and Huffman (1983), among others.

The only solid inclusions observed in the present flux-grown crystals are long-prismatic needles of rutile. As no broad band centered at 24 500 cm^{-1} has been observed in optical absorption spectra of Ti^{3+}-bearing rutile (e.g., Khomenko et al. 1998; Lu et al. 2001), and we do not observe in our spectra any traces of the strong and broad 12 500 cm^{-1} band recorded in spectra of blue rutile (Khomenko et al. 1998), it is highly unlikely that intrinsic absorption in submicroscopic rutile inclusions contributes to the broad bands observed for the flux-grown diopside crystals. To explore potential Mie-scattering effects, we have used the refractive indices for host (1.68) and inclusion (2.77) to calculate scattering curves for differently sized rutile inclusions in a pyroxene host. These calculations show that the presence of small (130–150 nm) rutile inclusions in pyroxene may cause a broad absorption maximum at 24 500 cm^{-1}. The calculations were based on the assumption of spherical rutile inclusions. The shape of rutile inclusions is normally prismatic and, consequently, it might be argued that this difference may influence the resulting scattering curves. However, a recent study by Munoz et al. (2006) indicated that scattering caused by small particles of rutile, which has a high real part of the refractive index, is not very sensitive to their shape. TEM imaging complemented by EDS analyses performed on several fragments of our flux-grown Ti^{3+}-bearing crystals showed no solid inclusions in this size range. The investigated fragments were in fact structurally and chemically homogenous down to the analytical resolution limit of the TEM-facility used (≤40 nm). In addition, the observed strong polarization of the 24 500 cm^{-1} band is difficult to explain in terms of scattering effects. Consequently, we find that Mie scattering does not present a reasonable explanation for the observed band at 24 500 cm^{-1} in the present spectra.

A further argument for an intrinsic electronic absorption process in the pyroxene structure as the cause for the 24 500 cm^{-1} band is its strong and consistent polarization. In the present spectra of flux-grown crystals, this broad band is strongly polarized in E||Y. The strong Y-polarization of the band consequently rules out an origin due to M1-M1 IVCT-processes, which are predicted to be strongly enhanced in E||**c**. An inventory of the various cation-cation vectors in the diopside structure (Table 3) shows that the M1-O2-T (Fig. 1) is the only one that has a crystallographic orientation suitable to host interacting cations to produce an IVCT band with strong E||Y-polarization in the present flux-grown diopside crystals. Although the overwhelming majority of observed IVCT bands in mineral spectra are caused by cations located at neighboring sites with common edges or faces (e.g., Amthauer and Rossman 1984), there are a small number of examples of IVCT-bands in mineral spectra assigned to charge transfer between cations at corner-sharing neighboring sites. For instance, Fe^{2+}-Ti^{4+} charge transfer has been observed in spectra of the rare mineral traskite (Mattson and Rossman 1988), in which Fe and Ti occupy corner-sharing octahedra. The broad IVCT band at ~20 000 cm^{-1} in spectra of schorlomite, which has been assigned to exchange processes between Fe^{2+} and Ti^{4+} at corner-sharing tetrahedral and octahedral sites (Locock et al. 1995), can serve as an additional example. The molar absorption coefficients for IVCT bands caused by transfer processes involving cations in corner-sharing coordination sites

TABLE 3. Cation distances and estimated relative absorbance values along different directions in the diopside structure (Clark et al. 1969), with **c** ∠ Z = 45°

Direction	Cation distance (Å)	Relative absorbance (%)				
		X	Y	Z	**c**	X+Y+Z
M1-M1	3.092	36	27	37	73	100
T-T	3.107	36	28	36	71	100
M1-T	3.214	4	0	96	30	100
	3.266	59	25	15	7	100
	3.476	25	66	10	2	100
Measured		30	54	16	13	100

are expected to be distinctly lower than for corresponding bands caused by processes among cations at edge- or face-sharing sites (Mattson and Rossman 1988). The low molar absorptivity of ca. 45 L^2/mol·cm recorded for the 24 500 cm^{-1} band in the present spectra is thus consistent with the proposed assignment.

On the basis of the broadness of the absorption band at 24 500 cm^{-1} in the present spectra, its strong E||Y-polarization, and the good correlation between its intensity and sample chemistry in terms of combined Ti^{3+} occupancy at M1-sites and Ti^{4+} occupancy at T-sites (Fig. 8c), we assign this band to a $^{M1}Ti^{3+}$-$^{T}Ti^{4+}$ intervalence charge transfer process.

ACKNOWLEDGMENTS

Margareta Sundberg and Kjell Jansson are thanked for TEM-imaging of selected single-crystal fragments. Financial support from the Swedish Research Foundation (VR) is greatly appreciated. We thank G.R. Rossman, B. Wopenka, and an anonymous referee for constructive reviews and comments that improved the manuscript.

REFERENCES CITED

Amthauer, G. and Rossman, G.R. (1984) Mixed valence of iron in minerals with cation clusters. Physics and Chemistry of Minerals, 11, 37–51.

Bohren, C.F. and Huffman, D.R. (1983) Absorption and scattering of light by small particles. John Wiley, New York.

Burns, R.G. and Huggins, F.E. (1973) Visible-region absorption spectra of a Ti^{3+} fassaite from the Allende meteorite: A discussion. American Mineralogist, 58, 955–961.

Clark, J.R., Appleman, D.E., and Papike, J.J. (1969) Crystal-chemical characterization of clinopyroxenes based on eight new structure refinements. Mineralogical Society of America Special Paper, 2, 31–50.

Dowty, E. and Clark, J.R. (1973a) Crystal structure refinement and optical properties of a Ti^{3+} fassaite from the Allende meteorite. American Mineralogist, 58, 230–242.

——— (1973b) Crystal structure refinement and optical properties of a Ti^{3+} fassaite from the Allende meteorite: Reply. American Mineralogist, 58, 962–964.

Goreva, J.S. and Rossman, G.R. (2000) A blue variety of rose quartz. Geological Society of America 2000 Annual Meeting, Reno, Nevada. GSA Abstracts with Programs, Vol. 32, November 2000.

Goreva, J.S., Ma, C., and. Rossman, G.R. (2001) Fibrous nanoinclusions in massive rose quartz: The origin of rose coloration. American Mineralogist, 86, 466–472.

Hålenius, U., Kristiansson, P., and Skogby, H. (2000) Boron substitution in diopside evaluated through ^{11}B nuclear reaction analysis. Physics and Chemistry of Minerals, 27, 681–688.

Khomenko, V.M., Langer, K., Rager, H., and Fett, A. (1998) Electronic absorption by Ti^{3+} ions and electron delocalization in synthetic blue rutile. Physics and Chemistry of Minerals, 25, 338–346.

Khomenko, V.M., Langer, K., Wirth, R., and Weyer, B. (2002) Mie scattering and charge transfer phenomena as causes of the UV edge in the absorption spectra of natural and synthetic almandine garnets. Physics and Chemistry of Minerals, 29, 201–209.

Kristiansson, P., Hålenius, U., Skogby, H., Elfman, M., Malmqvist, K., and Pallon, J. (1999) Boron distributions in single crystals investigated with nuclear reaction microanalysis. Nuclear Instruments and Methods in Physics Research, Section B, 158, 562–567.

Locock, A., Luth, R.W., Cavell, R.G., Smith, D.G.W., and Duke, M.J.M. (1995) Spectroscopy of the cation distribution in the schorlomite species of garnet. American Mineralogist, 80, 27–38.

Lu, T.C., Wu, S.Y., Lin, L.B., and Zheng, W.C. (2001) Defects in the reduced rutile single crystal. Physica, B304, 147–151.

Ma, C., Goreva, J.S., and Rossman, G.R. (2002) Fibrous nanoinclusions in massive rose quartz: HRTEM and AEM investigations. American Mineralogist, 87, 269–276.

Mao, H.K. and Bell, P.M. (1974) Crystal-field effects of trivalent titanium in fassaite from the Pueblo de Allende meteorite. Carnegie Institution Yearbook, 73, 488–497.

Mattson, S.M. and Rossman, G.R. (1987) Identifying characteristics of charge transfer transitions in minerals. Physics and Chemistry of Minerals, 14, 94–99.

——— (1988) Fe^{2+}-Ti^{4+} charge-transfer in stoichiometric Fe^{2+}, Ti^{4+}-minerals. Physics and Chemistry of Minerals, 16, 78–82.

Mie, G. (1908) Beiträge zur Optik trüber Medien, speziell kolloidaler Goldlösungen. Annalen der Physik, 25, 377–445.

Munoz, O., Volten, H., Hovenier, J.W., Min, M., Shkuratov, Y.G., Jalava, J.P., vand der Zande, W.J. and Waters, L.B.F.M. (2006) Experimental and computational study of light scattering by irregular particles with extreme refractive indeces: hematite and rutile. Astronomy and Astrophysics, 446, 525–535.

Nazzareni, S., Molin, G., Skogby, H., and Dal Negro, A. (2004) Crystal chemistry of Ti^{3+}-Ti^{4+}-bearing synthetic diopsides. European Journal of Mineralogy, 16, 443–449.

Ohashi, H., Fujita, T., and Osawa, T. (1982) The crystal structure of $NaTiSi_2O_6$ pyroxene. Journal of the Japanese Association of Mineralogists, Petrologists and Economic Geologists, 77, 305–309.

Pouchou, J.L. and Pichoir, F. (1984) A new model for quantitative X-ray microanalysis. I. Application to the analysis of homogeneous samples. La Recherche Aérospatiale, 3, 13–36.

Prewitt, C.T., Shannon, R.D., and White, W.B. (1972) Synthesis of pyroxene containing trivalent titanium. Contributions to Mineralogy and Petrology, 35, 77–82.

Quartieri, S., Antonioli, G., Artioli, G., and Lottici, P.P. (1993) XANES study of titanium coordination in natural diopsidic pyroxenes. European Journal of Mineralogy, 5, 1101–1109.

Redhammer, G.J., Ohashi, H., and Roth, G. (2003) Single-crystal structure refinement of $NaTiSi_2O_6$ clinopyroxene at low temperatures ($298 < T < 100$ K). Acta Crystallographica, B59, 730–746.

Skogby, H., Kristiansson, P., and Hålenius, U. (2003) An assessment of nuclear microprobe analyses of boron in silicate minerals. American Mineralogist, 88, 1601–1604.

Strens, R.G.J., Mao, H.K., and Bell, P.M. (1982) Quantitative spectra and optics of some meteoritic and terrestrial clinopyroxenes. In S.K. Saxena, Ed., Advances in physical geochemistry, p. 327–346. Springer Verlag, New York.

MANUSCRIPT RECEIVED NOVEMBER 17, 2005
MANUSCRIPT ACCEPTED JUNE 1, 2006
MANUSCRIPT HANDLED BY BRIGITTE WOPENKA